Fiber-distributed Ultra-wideband noise radar with steerable power spectrum and colorless base station

Jianyu Zheng,[1] Hui Wang,[1] Jianbin Fu,[2] Li Wei,[1] Shilong Pan,[2] Lixian Wang,[1] Jianguo Liu,[1,*] and Ninghua Zhu[1]

[1]*The State Key Laboratory on Integrated Optoelectronics, Institute of Semiconductors, Chinese Academy of Sciences, Beijing, 100083, China*

[2]*College of Electronic and Information Engineering, Nanjing University of Aeronautics and Astronautics, Nanjing, 210016, China*

[*]*jgliu@semi.ac.cn*

Abstract: A fiber-distributed Ultra-wideband (UWB) noise radar was achieved, which consists of a chaotic UWB noise source based on optoelectronic oscillator (OEO), a fiber-distributed transmission link, a colorless base station (BS), and a cross-correlation processing module. Due to a polarization modulation based microwave photonic filter and an electrical UWB pass-band filter embedded in the feedback loop of the OEO, the power spectrum of chaotic UWB signal could be shaped and notch-filtered to avoid the spectrum-overlay-induced interference to the narrow band signals. Meanwhile, the wavelength-reusing could be implemented in the BS by means of the distributed polarization modulation-to-intensity modulation conversion. The experimental comparison for range finding was carried out as the chaotic UWB signal was notch-filtered at 5.2 GHz and 7.8 GHz or not. Measured results indicate that space resolution with cm-level could be realized after 3-km fiber transmission thanks to the excellent self-correlation property of the UWB noise signal provided by the OEO. The performance deterioration of the radar raised by the energy loss of the notch-filtered noise signal was negligible.

OCIS codes: (060.5625) Radio frequency photonics; (350.4010) Microwaves; (190.3100) Instabilities and chaos; (280.5600) Radar.

References

1. D. Porcino and W. Hirt, "Ultra-wideband radio technology: Potential and challenges ahead," IEEE Commun. Mag. **41**(7), 66–74 (2003).
2. H. Sun, Y. Lu, and G. Liur, "Ultra-wideband technology and random signal radar: an ideal combination," IEEE Aerosp. Electron. Syst. Mag. **18**(11), 3–7 (2003).
3. C. Lai and R. M. Narayanan, "Ultrawideband random noise radar design for through-wall surveillance," IEEE Trans. Aerosp. Electron. Syst. **46**(4), 1716–1730 (2010).
4. S. C. Surender and R. M. Narayanan, "UWB noise-OFDM netted radar: Physical layer design and analysis," IEEE Trans. Aerosp. Electron. Syst. **47**(2), 1380–1400 (2011).
5. L. Illing and D. J. Gauthier, "Ultra-high-frequency chaos in a time-delay electronic device with band-limited feedback," Chaos **16**(3), 033119 (2006).
6. S. M. Han, O. Popov, and A. S. Dmitriev, "Flexible chaotic UWB communication system with adjustable channel bandwidth in CMOS technology," IEEE Trans. Microwave Theory Technol. **56**(10), 2229–2236 (2008).
7. M. I. Jeong, J. N. Lee, and C. S. Lee, "Design of quasi-chaotic signal generation circuit for UWB chaotic-OOK system," J. Electromagn. Waves Appl. **22**(13), 1725–1733 (2008).
8. F. Y. Lin and J. M. Liu, "Chaotic radar using nonlinear laser dynamics," IEEE J. Quantum Electron. **40**(6), 815–820 (2004).
9. J.-Y. Zheng, M.-J. Zhang, A.-B. Wang, and Y.-C. Wang, "Photonic generation of ultrawideband pulse using semiconductor laser with optical feedback," Opt. Lett. **35**(11), 1734–1736 (2010).
10. M.-J. Zhang, T.-G. Liu, A.-B. Wang, J.-Y. Zheng, L.-N. Meng, Z.-X. Zhang, and Y.-C. Wang, "Photonic ultrawideband signal generator using an optically injected chaotic semiconductor laser," Opt. Lett. **36**(6), 1008–1010 (2011).

#199697 - $15.00 USD Received 17 Oct 2013; revised 25 Jan 2014; accepted 30 Jan 2014; published 24 Feb 2014

11. L. X. Wang, N. H. Zhu, J. Y. Zheng, J. G. Liu, and W. Li, "Chaotic ultra-wideband radio generator based on an optoelectronic oscillator with a built-in microwave photonic filter," Appl. Opt. **51**(15), 2935–2940 (2012).
12. H.-J. Song, N. Shimizu, N. Kukutsu, T. Nagatsuma, and Y. Kado, "Microwave photonic noise source from microwave to sub-Terahertz wave bands and its applications to noise characterization," IEEE Trans. Microwave Theory Technol. **56**(12), 2989–2997 (2008).
13. J.-W. Shi, F.-M. Kuo, T. Chiueh, H.-F. Teng, H. J. Tsai, N.-W. Chen, and M.-L. Wu, "Photonic generation of millimeter-wave white-light at W-band using a very broadband and high-power photonic emitter," IEEE Photonics Technol. Lett. **22**(11), 847–849 (2010).
14. Y. Peled, M. Tur, and A. Zadok, "Generation and detection of Ultra-wideband waveforms using stimulated Brillouin scattering amplified spontaneous emission," IEEE Photonics Technol. Lett. **22**(22), 1692–1694 (2010).
15. T. Nagatsuma, T. Kumashiro, Y. Fujimoto, K. Taniguchi, K. Ajito, N. Kukutsu, T. Furuta, A. Wakatsuki, and Y. Kado, "Millimeter-wave imaging using photonics-based noise source," in *Proceedings of 34th International Conference on Infrared, Millimeter, and Terahertz Waves* (IEEE, 2009), pp. 1–2.
16. J. Yao, "Photonics for ultrawideband communications," IEEE Microwave Mag. **10**(4), 82–95 (2009).
17. J. E. Román, L. T. Nichols, K. J. Williams, R. D. Esman, G. C. Tavik, M. Livingston, and M. G. Parent, "Fiber-optic remoting of an ultrahigh dynamic range radar," IEEE Trans. Microwave Theory Technol. **46**(12), 2317–2323 (1998).
18. J. B. Fu and S. L. Pan, "Fiber-connected UWB sensor network for high-resolution localization using optical time-division multiplexing," Opt. Express **21**(18), 21218–21223 (2013).
19. D. Grodensky, D. Kravitz, and A. Zadok, "Ultra-wideband microwave-photonic noise radar based on optical waveform generation," IEEE Photonics Technol. Lett. **24**(10), 839–841 (2012).
20. M. Hämäläinen, V. Hovinen, R. Tesi, J. H. J. Iinatti, and M. Latva-aho, "On the UWB system coexistence with GSM900, UMTS/WCDMA, and GPS," IEEE J. Sel. Areas Commun. **20**(9), 1712–1721 (2002).
21. Fed. Commun. Commission, Revision of Part 15 of the Commission's Rules Regarding Ultra-Wideband Transmission Systems, Tech. Rep. ET-Docket 98–153, FCC02–48, Apr. (2002).
22. J. Zheng, N. Zhu, L. Wang, H. Wang, Y. Du, and J. Liu, "Photonics-assistant spectra shaping of ultra-wideband signals for dynamic spectrum access in cognitive network," Proc. SPIE **8552**, 85520H (2012).
23. J. Zheng, H. Wang, L. Wang, N. Zhu, J. Liu, and S. Wang, "Implementation of wavelength reusing upstream service based on distributed intensity conversion in ultrawideband-over-fiber system," Opt. Lett. **38**(7), 1167–1169 (2013).
24. T. Shao and J. Yao, "Wavelength reuse in a bidirectional UWB over fiber system," Opt. Express **21**(10), 11921–11927 (2013).
25. J. D. Bull, N. A. F. Jaeger, H. Kato, M. Fairburn, A. Reid, and P. Ghanipour, "40 GHz electro-optic polarization modulator for fiber optic communications systems," Proc. SPIE **5577**, 133–143 (2004).
26. M. W. Lee, L. Larger, V. Udaltsov, E. Genin, and J.-P. Goedgebuer, "Demonstration of a chaos generator with two time delays," Opt. Lett. **29**(4), 325–327 (2004).
27. M. Peil, M. Jacquot, Y. K. Chembo, L. Larger, and T. Erneux, "Routes to chaos and multiple time scale dynamics in broadband bandpass nonlinear delay electro-optic oscillators," Phys. Rev. E Stat. Nonlinear Soft Matter Phys. **79**(2), 026208 (2009).

1. Introduction

As an emerging technology, Ultra-wideband (UWB) radio has attracted a great deal of interest from academia, industry, and global standardization bodies due to its various advantages, such as immunity to multipath fading, low power consumption as well as high range resolution [1]. Meanwhile, Random signal radar is another type of newly-developed radar system. Its features include low probability of intercept, good range-Doppler resolution and so on [2]. As one kind of the UWB radars, the UWB noise radar was concerned continuously in the past few years because it combines the features of UWB radar and random signal radar [2]. The UWB noise radar for through-wall surveillance [3] or netted radar sensor system [4] has been proposed and demonstrated recently. In practice applications, the chaotic circuits are usually adopted to provide the UWB noise signal in the UWB noise radar [5–7]. In order to improve the performance of the UWB noise radar, the noise signal with higher bandwidth generated by photonics-assisted techniques was proposed [8–15]. In 2004, Lin and Liu demonstrated the chaotic-UWB radar where the photoelectric-converted noise signal output from the chaotic operated laser diode with optical injection [8]. Based on the chaotic dynamics of the laser diode and optoelectronic oscillator (OEO), a series of methods for UWB noise signal generation were proposed since 2010 [9–11]. The inherent random of the amplified spontaneous emission (ASE) light source has been utilized to generate the UWB noise signal at almost the same time [12–15]. Song *et al.* proposed a photonics-assisted technique to produce the UWB noise signal from the microwave to sub-terahertz region with an ASE light source, optical filter, and photodetector (PD) [12]. In order to generate the UWB signal with high power density in W-band (75-110 GHz), a near-

#199697 - $15.00 USD Received 17 Oct 2013; revised 25 Jan 2014; accepted 30 Jan 2014; published 24 Feb 2014

ballistic uni-traveling-carrier PD was used in the ASE based UWB noise source [13]. In [14], the ASE that is associated with stimulated Brillouin scattering (SBS), namely SBS-ASE, was also used to generate the UWB noise signal. The millimeter-wave imaging using ASE-based noise source was demonstrated in 2009 [15].

Except as a mean to enhance the bandwidth of the UWB signals, the photonics-assisted methods also could be adopted in the radio-over-fiber system to extend the coverage of the radar signal and establish the fiber-distributed radar networks [16]. In such fiber-distributed radar networks, generation of the probing signal and processing of mass-data are completed in the center station (CS), meanwhile, the remote base stations (BSs) with low cost are in charge of signal's transmitting and receiving [17, 18]. Recently, a fiber distributed UWB noise radar system was established, in which photonic UWB noise sources using the ASEs of both SBS and erbium doped fiber amplifiers were applied to provide the detected and referenced signals [19]. However, two issues should be considered in a practicable fiber-distributed UWB noise radar system, which have not been solved appropriately in [19]. The first one is how to avoid interference resulting from power spectrum overlay between the UWB signal and other existing narrowband (NB) radio signals. In order to avoid the interference to the Global Position System (GPS) and the traditional mobile communication systems [20], the Federal Communications Commission (FCC) already stipulated that the UWB signals only work in the range of 3.1–10.6 GHz, yet some other NB systems whose operated frequency bands locate in this range could not be immune to the interference totally [21]. The implicated NB communication systems include but not limited to the Wireless Fidelity (Wi-Fi) system operating at 5.2 GHz and the C-band satellite communication systems working at 7–8 GHz. Therefore, the generation of a photonic-assisted generation of the UWB signal with tunable notch band behavior becomes a highly significant solution since it can realize dynamic spectrum accessing at the CS according to the real-time environment for avoiding the spectrum-overlay-induced interference [22]. Unfortunately, the power spectra of the photonic UWB noise signal generated by the methods described in [8–15] are difficult to be controlled precisely for complying with the FCC indoor mask and avoiding the spectrum-overlay-induced interference to the NB communication systems. Another issue about the fiber-distributed UWB noise radar is how to implement the wavelength reusing at the BS, i.e. establish the colorless BS, which is the key problem for improving the networks compatibility and reducing the link cost. Recently, some methods have been demonstrated to establish an UWB-over-fiber link with colorless BS for indoor high-speed wireless communication [23, 24]. However, a fiber-distributed UWB noise radar system with colorless BS has not yet been achieved, which could be used to establish high-performance and low cost wireless sensor networks (WSN) in a particular location [4].

In this work, a fiber-distributed UWB noise radar is achieved, which consists of a chaotic OEO based UWB noise source, a fiber-distributed transmission link, a colorless BS, and a cross-correlation information processing module. The distributed polarization modulation-to-intensity modulation (PolM-to-IM) conversion is utilized in the UWB noise source and transmission link in order to implement power spectrum controlling and BS colorlessness. The experiment results indicate that the spectrum-overlay-induced interference to the Wi-Fi and C-band satellite communication systems could be avoided as the chaotic OEO worked at the state of dual-loops. The space resolution of the proposed radar is up to cm-level as the probing signal is delivered over a length of 3-km SMF. This paper is organized as follows. Firstly, we introduce and analyze the principle and performances of the PolM-to-IM convertor because it is the key device of the proposed radar. Then, the PolM-to-IM convertor based chaotic OEO with band-limited feedback is elaborated whereas it is applied in the UWB radar as the signal source to provide the FCC-compliant and controllable noise signal. Next, the principle about how to realize the colorless BS in our radar would be described. A proof-of-concept experiment about distance measurement is carried out finally as the OEO works in the case of single-loop and dual-loops.

#199697 - $15.00 USD Received 17 Oct 2013; revised 25 Jan 2014; accepted 30 Jan 2014; published 24 Feb 2014

2. Experiment setup and principle

2.1 Polarization modulation-to-Intensity modulation convertor

Since the distributed PolM-to-IM converter, as the key device of the proposed UWB radar, is used in the UWB noise source and transmission link, its principle will be elaborated as follow. Figure 1 shows the model and response curves of the distributed PolM-to-IM convertor. The convertor consists of a polarization modulator (PolM), a polarization controller (PC), a transmission medium, and a polarization beam splitter (PBS). The PolM is a special phase modulator that can support both TE and TM modes with opposite phase modulation indices [25].

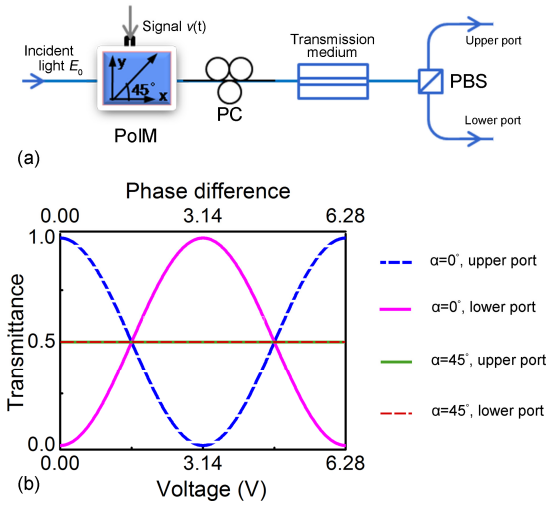

Fig. 1. (a) Equivalent model of the distributed PolM-to-IM convertor, PolM: Polarization modulator, PBS: polarization beam splitter, and (b) its transfer function curves.

As a linearly polarization optical carrier (OC) is injected into a PolM whose polarization direction is aligned to one principal axis of the PolM with an angle of 45°, the optical fields at the output port of the PolM along the two principal axes can be expressed as

$$\begin{bmatrix} E_x(t) \\ E_y(t) \end{bmatrix} = \frac{\sqrt{2}}{2} E_0 e^{j\omega_c t} \begin{bmatrix} e^{j(\beta V(t)+\varphi_0+\Delta\varphi)} \\ e^{-j\beta V(t)} \end{bmatrix} \tag{1}$$

where ω_c is the angular frequency of the OC, E_0 is the electrical field of incident light, φ_0 is a initial phase difference, $\Delta\varphi$ is additional phase shift induced by intermodal dispersion of the transmission medium, β is the phase modulation index, and $V(t)$ is the electrical field of the modulating signal. Hence, the optical field output from the upper and lower ports of the PBS will be expressed as

$$E_{upper}(t) = \cos(\pi/4+\alpha)\cdot E_x(t) + \cos(\pi/4-\alpha)\cdot E_y(t) \tag{2}$$

and

$$E_{lower}(t) = \sin(\pi/4-\alpha)\cdot E_x(t) - \sin(\pi/4+\alpha)\cdot E_y(t) \tag{3}$$

where α is the angle between the polarization direction of the OC and the principal axis of the upper port of the PBS. When the angle α is set at 0°, the optical fields output from the two ports of the PBS are given by

$$E_{upper}(t) = E_0 \exp(j(w_c t + (\varphi_0+\Delta\varphi)/2))\cos(\beta V(t) + (\varphi_0+\Delta\varphi)/2) \tag{4}$$

#199697 - $15.00 USD Received 17 Oct 2013; revised 25 Jan 2014; accepted 30 Jan 2014; published 24 Feb 2014

and

$$E_{lower}(t) = E_0 \exp(j(w_c t + (\varphi_0 + \Delta\varphi)/2 + \pi/2))(\sin(\beta V(t) + (\varphi_0 + \Delta\varphi)/2) \quad (5)$$

The nonlinear transfer functions of the PolM-to-IM convertor is, therefore, described as

$$T_{upper}(t) = \left|E_{upper}(t)\right|^2 / \left|E_0 e^{jw_c t}\right|^2 = 1/2 \cdot (1 + \cos(2\beta V(t) + \varphi_0 + \Delta\varphi)) \quad (6)$$

and

$$T_{lower}(t) = \left|E_{upper}(t)\right|^2 / \left|E_0 e^{jw_c t}\right|^2 = 1/2 \cdot (1 - \cos(2\beta V(t) + \varphi_0 + \Delta\varphi)) \quad (7)$$

which were plotted in Fig. 1(b). Obviously, the polarity-inverted intensity optical signal will output from the two ports of the convertor while any electrical signal is applied on the PolM. Moreover, as φ is set to be $\pi/2$ by adjusting the PC or changing the bias voltage of the PolM (φ is the sum of φ_0 and $\Delta\varphi$, called as static phase difference), for $\beta \ll 1$, $\sin(2\beta V(t)) \approx 2\beta V(t)$, thus the transfer function can be rewritten as

$$T_{upper}(t) = 1/2 + \beta V(t) \quad (8)$$

and

$$T_{lower}(t) = 1/2 - \beta V(t) \quad (9)$$

From Eqs. (8) and (9), it can be seen that the modulated signal will be recovered without any distortion by the convertor.

As α is fixed into ± 45° by the PC, the optical fields output from the PBC are E_x and E_y. Obviously, only the phase of the OC is modulated, and the amplitude will keep constant. Therefore, the response curve of the convertor is a line in this case, as shown in the Fig. 1(b), which means that the OC could be re-modulated by an intensity modulator (IM) in order to implement the wavelength reusing.

2.2 Nonlinear OEO based noise source

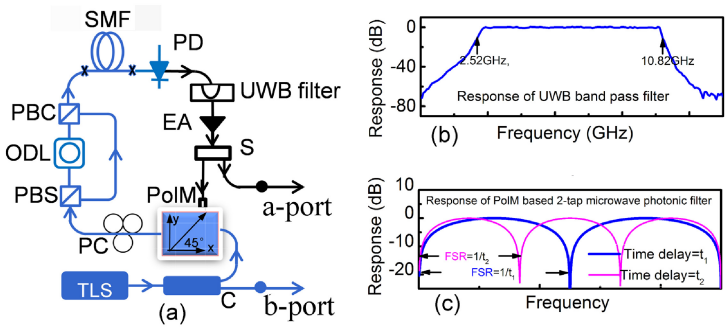

Fig. 2. (a) Experimental setup of the PolM based OEO with dual-loops, TLS: tunable laser source, C: optical coupler, PolM: polarization modulator, PBS: polarization beam splitter, ODL: optical delay line, PBC: polarization beam combiner, SMF: single mode fiber, PD: photodetector, UWB filter: ultra-wide band filter, EA: electrical amplifier, S: electrical splitter, (b) the response curve of the UWB band pass filter used in the feedback loop of the OEO and (c) the simulated response curve of the PolM based two-taps MPF used in the OEO.

Figure 2(a) shows the experimental setup of the polarization modulation based dual-loops nonlinear OEO where a PolM-to-IM convertor is applied in the feedback loop. A linearly polarized light output from a tunable laser source (TLS) is introduced into a 40-GHz PolM which is embedded to the delayed feedback loops of the OEO functions as a fast electrical-to-optical convertor. A polarization maintaining fiber (PMF) is used between the TLS and PolM to make sure the polarization direction of the injected input light is with an orientation angle of 45° to one principal axis of the PolM. The polarization state of the input light is thus

#199697 - $15.00 USD Received 17 Oct 2013; revised 25 Jan 2014; accepted 30 Jan 2014; published 24 Feb 2014

modulated according to the voltage applied to the PolM. The PC is employed between the PolM and the PBS to align the polarization direction of input light oriented to one principal axes of the PBS, i. e. $\alpha = 0$, for implementing PolM-to-IM conversion. The obtained intensity modulated lights from the two output ports of the PBS are combined again by the polarization beam combiner (PBC) with time delay difference (TDD) $\Delta\tau_D$ provided by the optical delay line (ODL). The combined light is sent into the single mode fiber (SMF), in which the light experiences a large time delay τ_D. Subsequently, the optical signal is converted into a radio frequency (RF) signal by a PD with a bandwidth of 18 GHz. An electronic UWB filter with a pass band from 2.52 GHz to 10.82GHz displayed in Fig. 2(b) is connected after the PD as a band-limited electronic component. The spectrum filtered electrical signal is then amplified by using a broadband electrical amplifier with a max gain of 30 dB and bandwidth from 100 kHz to 20 GHz. The amplified RF signal is used to drive the PolM. An electrical splitter (S) and an optical coupler (C) are used to output the electrical signal and the light from the OEO. In general, the dynamics for this kind of setup can be described by a delay differential equation (DDE) with two time delays [26]

$$x + \tau\frac{dx}{dt} = mT_{upper}(x(t-\tau_D)) + mT_{lower}(x(t-(\tau_D + \Delta\tau_D)), \tag{10}$$

where $\tau = 1/2\pi f_H$ is the characteristic time scale of the high-frequency cutoff, m is the normalized gain in the loop. Due to the bandpass property of the UWB filter, the low-frequency cutoff in the feedback loop could not be neglected. According to the Ref [5, 27], the modified DDE for this band-limited system is presented as

$$\begin{aligned}(1+\frac{\tau}{\theta})x + \tau\frac{dx}{dt} + \theta^{-1}\int_{t_0}^{t} x(s)ds = \\ mT_{upper}(x(t-\tau_D)) + mT_{lower}(x(t-(\tau_D + \Delta\tau_D))\end{aligned}, \tag{11}$$

where $\theta = 1/2\pi f_L$ denotes the characteristic time scale of the low-frequency cutoff. The integral term comes from the bandpass property of the UWB filter. When the feedback gain is high enough, the nonlinear OEO will fall into broadband chaotic oscillation. As the nonlinear OEO operates with single-loop, the chaotic-UWB signals with flat power spectrum could be generated [27]. Moreover, the chaotic UWB signal will be FCC-compliant because of the band limitation of the UWB filter employed in the loop. However, the Eq. (11) cannot present intuitively the frequency domain characteristics of the chaotic signal output from the dual-loops OEO. As a matter of fact, the two signals, after synthesizing by the PBC, will not interfere with each other in the SMF because of the mutually orthogonal property when both arms are kept closing. Therefore, this dual-loops OEO could be equivalent to two independent single-loop OEOs in nature. These two OEOs share almost identical feedback link and are with the same parameters except the delay time τ_D. Due to the complementarity between the transfer functions of the PolM-to-IM convertor (See Fig. 1(b)), the inverted signals will generated simultaneously at the upper and lower arms. As shown in Fig. 2(c), a negative coefficient microwave photonic filter (MPF) is formed in the feedback loop, whose transfer function is given by

$$H(f) = a - a\cdot\exp(-j2\pi f\Delta\tau_D), \tag{12}$$

where f denotes the signal frequency, a is the tap coefficient, $\Delta\tau_D$ is the TDD and corresponds to basic delay of the filter. It can be seen from Fig. 2(c) that the notch frequency appears periodically and the free spectral range (FSR) has a reverse relation to the TDD. So, by adjusting the TDD, a chaotic-UWB signal with tunable notch filtering could be generated. It is worth noting that a relative long SMF (8-km) was applied in our experiment since longer fiber delay corresponds to lower feedback gain for generating a band-limited chaotic signal [11].

#199697 - $15.00 USD Received 17 Oct 2013; revised 25 Jan 2014; accepted 30 Jan 2014; published 24 Feb 2014

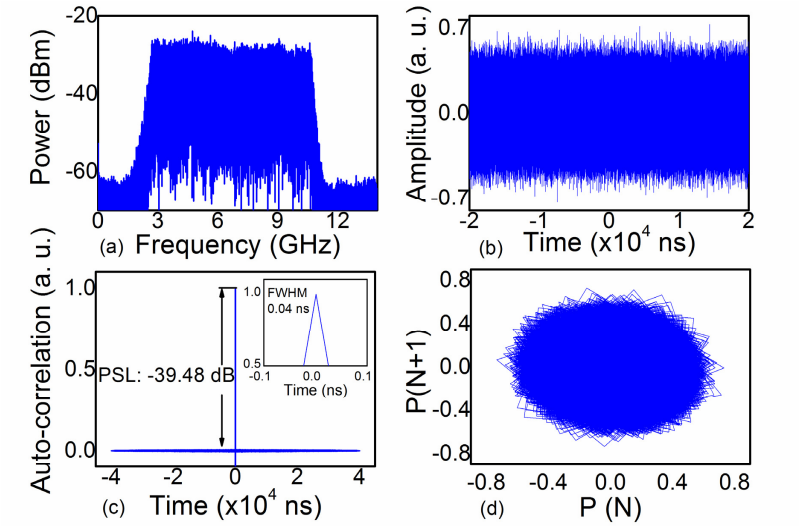

Fig. 3. Power spectra (a), time sequence (b), auto-correlation trace (c), and phase portrait (d) of the UWB noise signals output from the chaotic OEO with single-loop.

When only one arm was closed, a chaotic-UWB signal was measured at the output of the OEO by increasing the loop gain progressively. Figures 3(a)–3(d) show the power spectra, time sequence, auto-correlation trance, and phase portrait of the UWB noise signal output from the chaotic electro-optic oscillator. As shown in Fig. 3(a), the UWB noise signal with flat power spectra were generated, as expected, whose spectra shape is in accord with the response curve of the UWB filter. Hence, the center frequency and 10-dB bandwidth of the noise signal are 6.67 GHz and 8.30 GHz, respectively. A narrow spike could be seen in the autocorrelation trace with a measurement time window of 40 μs. The peak sidelobe level (PSL) of –39.48 dB is low enough for the application of the chaotic signal in the UWB noise radar system. The full width at half maximum (FWHM) of the correlation peak is 0.04 ns. Meanwhile, there is no discernible structure in the phase portrait which is an indication of high-dimensional chaos [5, 8] (See Fig. 3(d)).

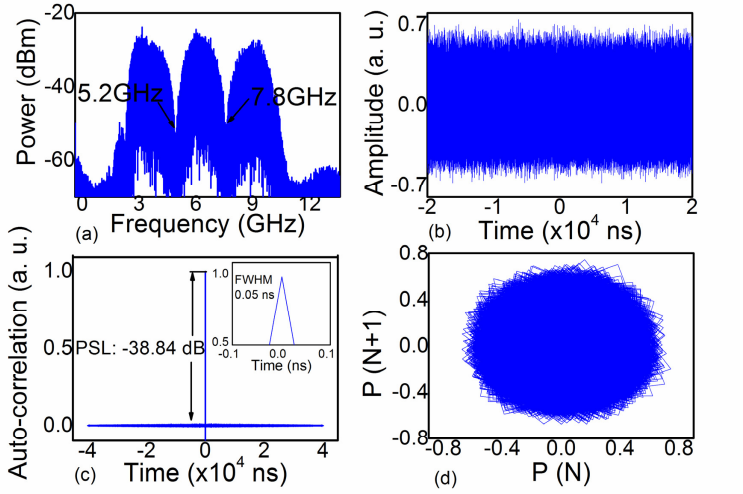

Fig. 4. Power spectra (a), time sequence (b), auto-correlation trace (c), and phase portrait (d) of the UWB noise signals output from the chaotic OEO with dual-loops ($\Delta\tau_D$ = 384.6 ps).

#199697 - $15.00 USD Received 17 Oct 2013; revised 25 Jan 2014; accepted 30 Jan 2014; published 24 Feb 2014

In order to investigate the performance of the chaotic OEO as it works with dual-loops, the generated signal was measured and processed. As the TDD was set at 384.6 ps, the power spectra, time sequence, auto-correlation trance, and phase portrait of the generated signal were displayed in Figs. 4(a)–4(d). It can be seen from Fig. 4(a) that two notches occurred at 5.2 GHz and 7.8 GHz raised by the notch-filtering effect of the MPF formed in the feedback loop. The energy losses of the signal at the notch-filtering positions induced that PSL and FWHM of the autocorrelation trace were decreased and increased to −38.84 dB and 0.05 ns respectively as displayed in Fig. 4(c). However, the phase portrait without any discernible structure implies that the OEO still operated in chaos state (See Fig. 4(d)). Moreover, the spectrum-overlay-induced interference to Wi-Fi and C-band satellite communication systems will be avoided if the OEO with dual-loops is applied in the UWB noise radar.

2.3 Fiber-distributed UWB radar with colorless base station

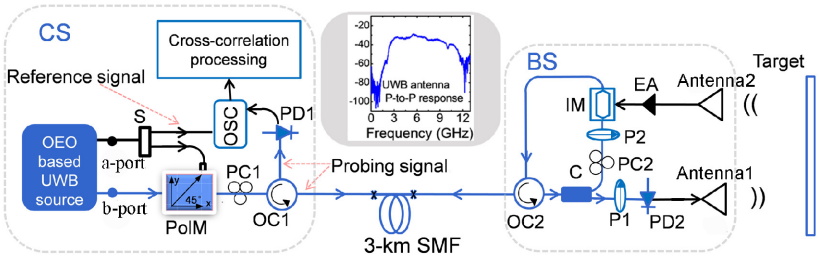

Fig. 5. Experiment setup of the fiber-distributed UWB noise radar with colorless base station, PolM: polarization modulator, OC: optical circulator, SMF: single mode fiber, C: optical coupler, P: polarizer, PD: photodetector, EA: electrical amplifier, IM: intensity modulator, OSC: oscilloscope, S: electrical splitter. Inset: response curve of the UWB antenna (point-to-point)

The PolM based OEO described in Section 2.2 is applied as signal source in the proposed fiber-distributed UWB noise radar with colorless BS. As illustrated in Fig. 5, the proposed radar consists of an UWB noise source, a 3-km fiber-distributed transmission link, a colorless base station based on the PolM-to-IM conversion, and a cross-correlation information processing module, whose operational principle is elaborated as follow.

The electrical UWB noise signal output from a-port of the chaotic OEO is split into two signals which are called as reference signal and probing signal. The electrical probing signal is applied on the PolM in the form of small signal modulation ($\beta \ll 1$) to modulate the linearly polarized OC output from b-port of the OEO. After transmitting in a 3-km SMF, the polarization modulated light is split into two beams by the 50/50 C in the BS. The two light beams are sent into the polarizer 1 and 2 (P1 and P2), whose polarization states will be controlled by the polarization controllers (PC1 and PC2) respectively. The probing signal will be recovered without distortion after the P1 while the angle α is set to 0° by controlling the PC1 and the static phase difference φ is set to be $\pi/2$ by adjusting the bias voltage of the PolM. The electrical probing signal converted by the PD2 are transmitted and received by a pair of UWB antennas whose response curve is shown in the inset of Fig. 5. Meanwhile, the second beam without any intensity fluctuation outputs from the P2 as the angle α is set to 45° by adjusting the PC2. The light outputs from the P2 is re-modulated with the received probing signal by the IM and transmitted to the center station (CS) via the 3- km SMF. Finally, the received probing signal is recovered again by the PD1. The reference and probing signals are recorded simultaneously with a 16-GHz real-time oscilloscope (OSC). Object detection and localization are accomplished through cross-correlation operation. Signal processing and data analysis are performed on a personal computer. The OEO based noise signal source could work with single-loop or dual-loops as required if the radar with colorless station is applied in practice. Utilizing the tunability of the MPF formed in the OEO's gain loop, the spectrum-

#199697 - $15.00 USD Received 17 Oct 2013; revised 25 Jan 2014; accepted 30 Jan 2014; published 24 Feb 2014

overlay-induced interference between UWB and NB signals could be avoided dynamically when the OEO works with dual-loops.

3. Proof-of-concept experiment

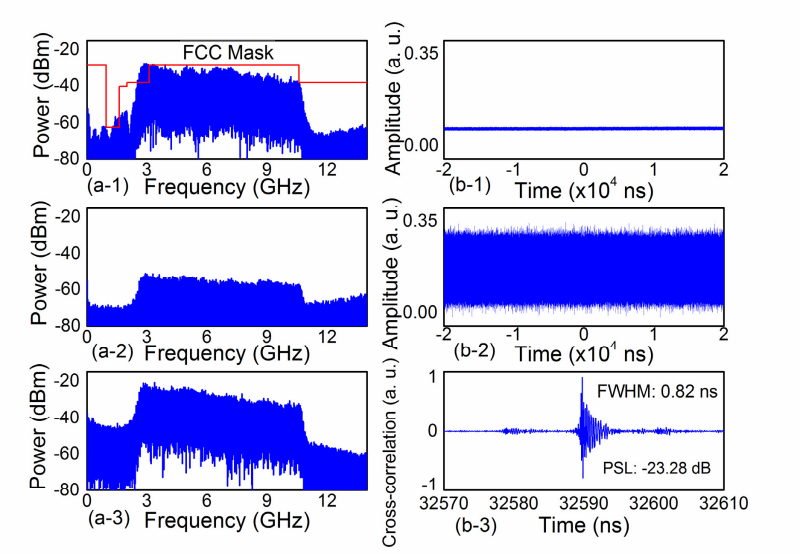

Fig. 6. Power spectra of the probing signals recorded after the PD2 (a-1), the antenna 2 (a-2), and the EA (a-3), the time sequence of the reused light detected by the PD1 as it is without (b-1) or with (b-2) the modulation from the IM, the cross-correlation trace between the probing and reference signals (b-3). All the results were recorded as the OEO worked with single-loop and the antenna 1 was pointed to the antenna 2 directly without any separation.

In order to investigate the link performance, the signals delivered between the CS and BS were measured and analyzed as the OEO worked with single-loop. To minimize the effect of loss and noise, all of the test results were obtained by pointing the antenna 1 to the antenna 2 directly without any separation. The power spectra of the probing signals recorded after the PD2, antenna 2, and EA is described in Figs. 6(a-1), 6(a-2), and 6(a-3) respectively. Comparing with the original UWB signal output by the OEO, the noise of the EA and the uneven gain of antennas induce the distortion of the signal in some degree. As shown in Fig. 6(a-1), the FCC-compliant UWB noise signal was recovered and emitted at the antenna 1 due to the distributed PolM-to-IM conversion. Figures 6(b-1) and 6(b-2) illustrate the time sequences of the reused light with or without re-modulation of the probing signals by the IM, which indicate the wavelength reusing were realized in the BS successfully. By cross-correlating the probing and reference signals, the FWHM of the correlation peak as shown in Fig. 6(b-3) is measured to be 0.82 ns. Deriving from this result, a high range resolution of 13.0 cm was demonstrated experimentally. The PSL is up to –23.38 dB.

Switching the OEO's work state from "single-loop" to "dual-loops" ($\Delta\tau_D$ = 384.6 ps) and keeping other conditions unchanged, all the results were recorded again, which are displayed in Fig. 7. It can be seen from Fig. 7(a) that the UWB signal with two notches at 5.2 GHz and 7.8 GHz were recovered, detected and amplified in the BS. Comparing with the "single-loop" state, the FWHM of the correlation peak increased to 1.16 ns. Correspondingly, the range resolution reduced to 17.4 cm in this case. Meanwhile, the PSL also reduced to –20.20 dB. Although the signal performance of the proposed radar is degraded as the OEO works with dual-loops due to the energy losses of the probing signal, the spectrum-overlay-induced interference to the Wi-Fi and C-band satellite communication systems could be avoided.

#199697 - $15.00 USD Received 17 Oct 2013; revised 25 Jan 2014; accepted 30 Jan 2014; published 24 Feb 2014

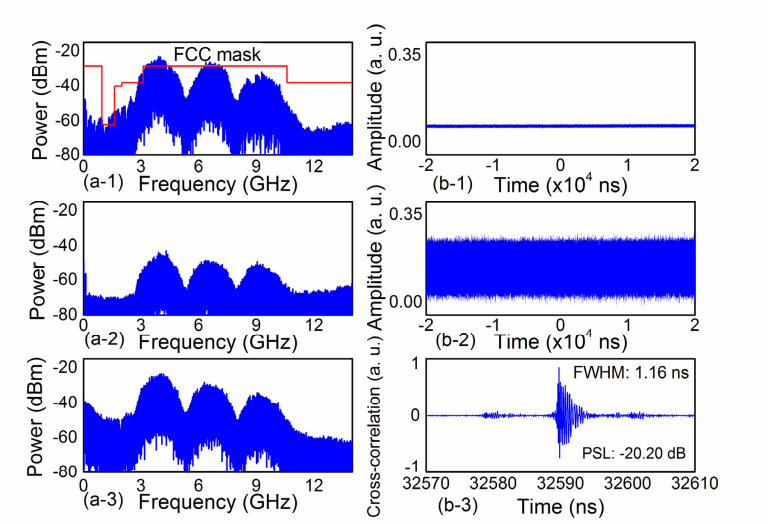

Fig. 7. Power spectra of the probing signals recorded after the PD2 (a-1), the antenna 2 (a-2), and the EA (a-3), the time sequence of the reused light detected by the PD1 as it is without (b-1) or with (b-2) the modulation from the IM, the cross-correlation trace between the probing and reference signals (b-3). All the results were recorded as the OEO worked with dual-loops ($\Delta\tau_D$ = 384.6 ps) and the antenna 1 was pointed to the antenna 2 directly without any separation.

A proof-of-concept experiment was performed to demonstrate the ability of the distributed radar in range finding as the OEO based signal source worked with single-loop or dual-loops ($\Delta\tau_D$ = 384.6 ps). In this experiment, a 35 cm × 26 cm metal plate was regarded as the target. The antennas faced the same direction and were separated with 10 cm horizontally to eliminate the crosstalk. The cross-correlation traces with the target 15, 75, and 225 cm away from the antennas are displayed in the Figs. 8(a) and 8(b). As can be seen, the peaks indicating the location of the target can be identified unambiguously whether the OEO based signal source worked with single-loop or dual-loops. We measured the FWHM and PSL of the cross-correlation traces as the distance between the antennas and target was 225 cm. In the case of single-loop, the FWHM and PSL were 1.46 ns (21.9 cm) and −12.42 dB respectively. They increased to 1.86 ns (27.9 cm) and −11.55 dB as the signal source worked with dual-loops. The interference from the other wireless systems and multipath effect induced the performance degradation of the fiber-distributed UWB noise radar. Figure 8 indicates that the measured result had no severe deterioration in the experiment as the probing signal was notch-filtered at 5.2 GHz and 7.8 GHz, which proofs that the notch-filtered UWB noise signal could be applied in practice directly in order to avoid the spectrum-overlay-induced interference to the Wi-Fi and C-band satellite communication systems. To have a better performance for this proposed radar, the higher amplified probing signal and more optimized algorithm are desired.

#199697 - $15.00 USD Received 17 Oct 2013; revised 25 Jan 2014; accepted 30 Jan 2014; published 24 Feb 2014

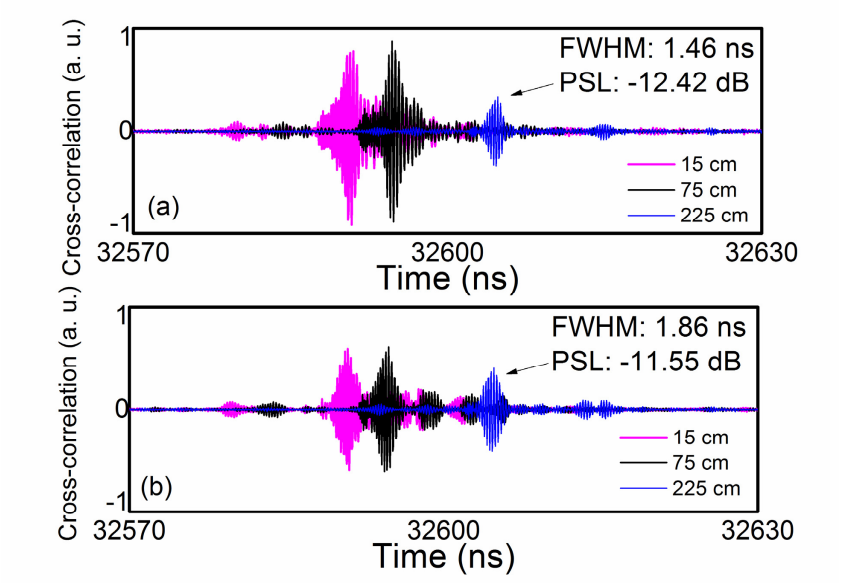

Fig. 8. Cross-correlation traces with the target 15, 75, and 225 cm away from the antennas, respectively. OEO worked with single-loop (a) and dual-loops ($\Delta\tau_D$ = 384.6 ps) (b).

4. Discussion and conclusion

In our experiment, the notch position of the probing signal could be changed according to the experiment demand through adjusting the TDD, which means that the interference to other NB wireless communication systems could be avoided dynamically. In addition, the phase variation inhered in the reused light will convert to intensity fluctuation due to the chromatic dispersion of the transmission link when the length of fiber used for distributing the probing signal is increased. The intensity fluctuation will be received by the PD1 in the CS together with the probing signal and impact the performance of the radar. However, this problem could be solved if an electroabsorption modulator (EAM) is used to replace the structure of the PC2, the P2, and the IM illustrated in the Fig. 5 for modulating the two orthogonal components of the reused light, because the intensity fluctuations in the both orthogonal directions converted from phase variations is complementary and could be cancelled out [24]. Moreover, the application of the EAM also could further reduce the complexity and cost of the BS. In addition, a commercial product for automatic polarization tracing and controlling could be adopted to increase the stability of the radar once it is applied in practice.

In conclusion, a fiber-distributed UWB noise radar were proposed and experimentally demonstrated by means of polarization modulation technique. In this proposed radar, a chaotic OEO was applied as the noise source. A PolM based two-taps MPF and an electrical UWB passband filter are embedded into the feedback loop of the OEO for shaping the power spectrum of the chaotic UWB signal. In the transmission link of the radar, the distributed PolM-to-IM convertor was used to implement the wavelength reusing in the CS. Finally, the radar with decimetre-level space resolution was experimentally demonstrated, whose sensing distance are more than 3-km. The center frequency and 10-dB bandwidth of the radar are 6.67 GHz and 8.30 GHz, which depend on the transfer function of the UWB filter inserted in the feedback loop of the chaotic OEO. The measured results indicated that the spectrum-overlay-induced interference to the NB communication systems could be avoided as the chaotic OEO worked in the state of dual-loops due to the microwave photonic notch filtering effect, although the performance of the radar was degraded in some degree comparing with the state of single-loop. Such findings are of great potential for future applications in the low-

#199697 - $15.00 USD Received 17 Oct 2013; revised 25 Jan 2014; accepted 30 Jan 2014; published 24 Feb 2014

cost UWB-over-fiber based WSN, which is compatible with WDM-PON and interference-free with the NB wireless systems.

Acknowledgments

This work was supported in part by the Major Program of the National Natural Science Foundation of China under Grant 61090390, by the National Basic Research Program of China under Grant 2012CB315702 and 2012CB315703, by the Foundation for Innovative Research Groups of the National Natural Science Foundation of China under Grant 61021003, by the Funds for International Cooperation and Exchange of the National Natural Science Foundation of China under Grant 60820106004, and by the Chinese Academy of Sciences (CAS) Special Grant for Postgraduate Research, Innovation, and Practice.

#199697 - $15.00 USD Received 17 Oct 2013; revised 25 Jan 2014; accepted 30 Jan 2014; published 24 Feb 2014